ACS OMEGA

http://pubs.acs.org/journal/acsodf

Article

Poly(vinyl alcohol)-Modified Membranes by $Ti_3C_2T_x$ for Ethanol Dehydration via Pervaporation

Weibin Cai,* Xue Cheng, Xiaohan Chen, Jiding Li, and Junqi Pei

Cite This: *ACS Omega* 2020, 5, 6277−6287

Read Online

ACCESS | Metrics & More | Article Recommendations

ABSTRACT: In this paper, PVA/$Ti_3C_2T_x$ mixed matrix membranes (MMMs) were prepared by mixing the synthesized $Ti_3C_2T_x$ with the PVA matrix, and the pervaporation (PV) performance of the ethanol−water binary system was tested. The morphology, structural properties, and surface characteristics of the membranes were investigated by scanning electron microscopy, atomic force microscopy, Fourier transform infrared spectroscopy, X-ray diffraction, degree of swelling, and water contact angle. The PVA/$Ti_3C_2T_x$ MMMs exhibit excellent compatibility and swelling resistance. Moreover the effects of the $Ti_3C_2T_x$ filling level, feed concentration, and operating temperature on the ethanol dehydration performance were systematically studied. The results demonstrated that the separation factor of PVA/$Ti_3C_2T_x$ MMMs was significantly increased because of $Ti_3C_2T_x$ promoting the cross-linking density of the membrane. Specifically, the membrane showed the best PV performance when $Ti_3C_2T_x$ loading was 3.0 wt %, achieving a separation factor of 2585 and a suitable total flux of 0.074 kg/m^2 h for separating 93 wt % ethanol solution at 37 °C.

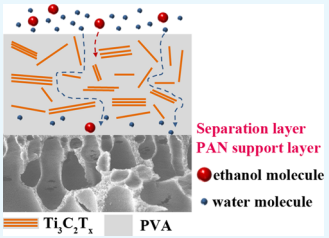

1. INTRODUCTION

Fuel ethanol,[1,2] as a renewable bioliquid fuel to reduce air pollution and greenhouse gases, has been promoted and used in many countries and regions around the world in recent years. With the severe environmental pollution and the exhaustion of resources such as petroleum, fuel ethanol has grown into one of the considerable alternative energy sources. One of the main production technologies of fuel ethanol is the biofermentation method,[3] which produces 6−10 wt % ethanol and then obtains 95 wt % industrial ethanol by distillation. To acquire absolute ethanol, particular methods must be adopted. Different from traditional separation methods, pervaporation (PV) technology[4] breaks the restriction of the vapor−liquid equilibrium and shows obvious advantages in the separation of liquid mixtures of azeotrope or close boiling compounds: energy conservation, environmental protection, less space, and easy for industrial scale-up.[5,6] The industrial application of the PV process has been widely recognized in organic solvent dehydration.[7,8] Many hydrophilic polymer membranes such as chitosan (CS),[9] poly(vinyl alcohol) (PVA),[10] sodium alginate (SA),[11] and so forth. have been investigated for the ethanol−water binary system. PVA possesses extraordinary physicochemical properties and can maintain its properties within long-term operation, which is suitable for providing basic membrane materials for organic solvent dehydration.[12] In 1982, the German GFT Company was the first to make breakthroughs in the industrial application of PV, introducing commercial PVA/poly(acrylonitrile) (PVA/PAN) composite membranes. However, a large number of OH groups in the PVA molecular chain result in strong hydrophilicity. Untreated PVA tends to swelling in aqueous solution, and the defects impair the separation performance of the PVA membrane.[13,14] The German GFT Company published the PV performance of the GFT commercial membrane: for 80 wt % ethanol aqueous mixture of the feed liquid, the separation factor was 100−200 and the total flux was 1.0 kg/m^2 h at 80 °C. In addition, the separation factor of the GFT-1510/2510 commercial membrane (95 wt % ethanol concentration) was 258 and the corresponding total flux was 0.6 kg/m^2 h.[15] Although the pristine PVA membrane has achieved industrial applications, its separation factor is still restricted. In order to combat this, many modification methods such as cross-linking,[16] grafting,[17] and blending[13] have been employed. Among them, doping two dimensional (2D) materials,[18] such as graphene,[19] graphene oxide (GO),[19,20] carbon nitride (C_3N_4),[21,22] metal−organic frameworks (MOFs),[23] and molybdenum disulfide (MoS_2), has attracted the attention of researchers.[24] In the work of Wu et al.,[25] various UiO membranes were fabricated by altering the organic linkers and doped in the PVA matrix for separation of 90 wt % ethanol solution. The mixed matrix membranes (MMMs) displayed obvious anti "trade-off" effects: for the UiO-66-$(OH)_2$/PVA-1.0 MMM, the total flux and separation factor were increased by 16 and 14%, respectively. Zhang and Wang[26] fabricated PVA/ZIF-8-NH_2 membranes for ethanol

Received: October 11, 2019
Accepted: March 10, 2020
Published: March 20, 2020

https://dx.doi.org/10.1021/acsomega.9b03388
ACS Omega 2020, 5, 6277−6287

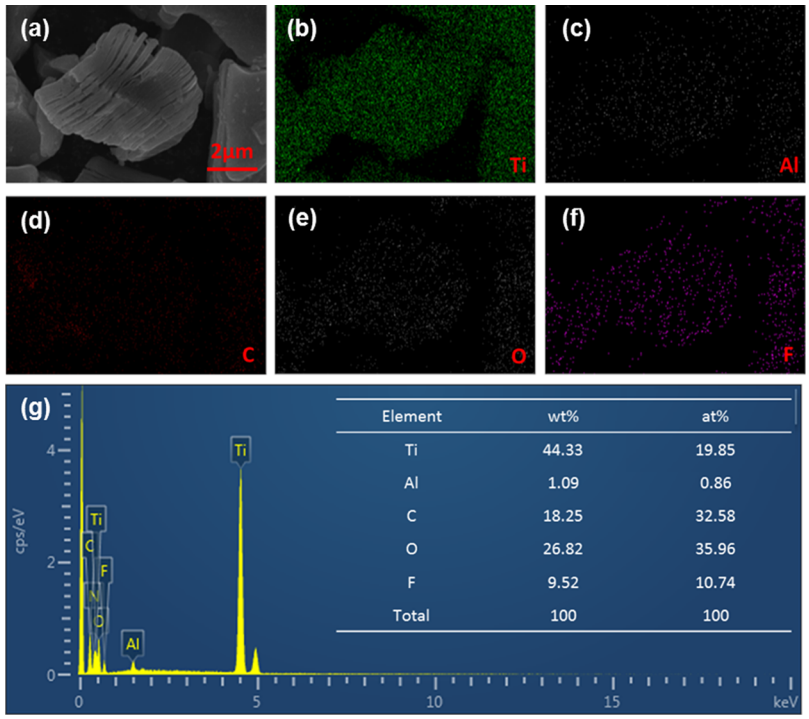

Figure 1. SEM images (a) and EDS results (b–g) of the $Ti_3C_2T_x$ powder.

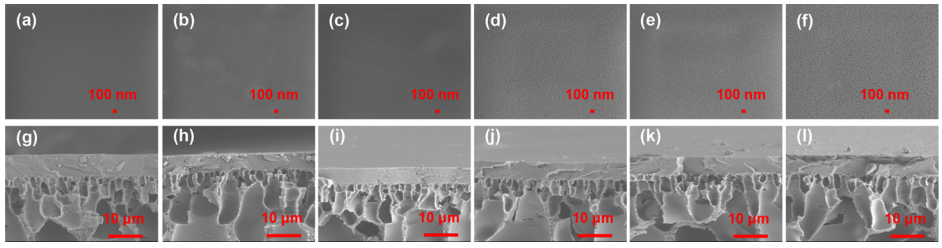

Figure 2. SEM surface view (a–f) and cross-sectional structure (g–l) of PVA/$Ti_3C_2T_x$ MMMs with different $Ti_3C_2T_x$ fillings: (a,g) 0.0; (b,h) 0.5; (c,i) 1.0; (d,j) 2.0; (e,k) 3.0; and (f,l) 4.0 wt %.

dehydration. The MMMs exhibited enhanced PV performance, which was due to the increased hydrophilicity of ZIF-8-NH_2 with the PVA matrix. The total flux and separation factor of PVA/ZIF-8-NH_2 MMMs could reach to 0.13 kg/m^2 h and 201, respectively, at 40 °C.

2D materials[27] with atomic thickness and micrometer lateral dimensions have been widely used to develop membranes with high separation performance. Moreover, they have mechanical properties, thermal stability, excellent layered structure, and 2D nanochannels, making the two-dimensional material separation membrane have extraordinary permeability.[28−30] As a new member of the 2D material family, transition metal carbides (MXenes) were discovered by Gogotsi and Barsoum in 2011. MXenes[31] have the formula $M_{n+1}X_nT_x$, where n is 1, 2, or 3, M is an early transition metal, X is C and/or N, and T is the OH and/or O group. Among them, the formula of MAX phases (the precursors of MXenes) is $M_{n+1}AX_n$, where A stands for an A-group element (such as Al and Si).[32] One of the most representative MAX materials is Ti_3AlC_2. Here, Al was extracted from Ti_3AlC_2[31,33] and a two-dimensional material called $Ti_3C_2T_x$ Mxene was prepared. The hydrophilic, rigorous layered structures and extremely short water molecule transport channel of $Ti_3C_2T_x$ have attracted the attention of researchers in the field of membrane separation.[34−37] Liu et al.[37] first prepared ultrathin $Ti_3C_2T_x$ membranes for desalination by assembling the $Ti_3C_2T_x$ nanomaterial. The selected $Ti_3C_2T_x$ membrane showed high water flux and salt rejection. In addition, this $Ti_3C_2T_x$ assembly membrane could maintain 100 h of PV desalination. Wu et al.[38] fabricated 2 μm-thick MXene membranes and applied it in ethanol dehydration. At room temperature and 5 wt % H_2O concentration, the total flux of the MXene membrane was 263 g m^{-2} h^{-1} and the separation factor was 135. At present, the $Ti_3C_2T_x$-based membrane has achieved some research results in terms of water treatment and gas separation.[39,40] Moreover, research studies on dehydration of organic solvents are still in progress.

Herein, for the first time, 2D $Ti_3C_2T_x$ was embedded in the PVA matrix, and PVA/$Ti_3C_2T_x$ MMMs was successfully prepared. Various membranes were labeled PVA/$Ti_3C_2T_x$-0.0, PVA/$Ti_3C_2T_x$-0.5, PVA/$Ti_3C_2T_x$-1.0, PVA/$Ti_3C_2T_x$-2.0, PVA/$Ti_3C_2T_x$-3.0, and PVA/$Ti_3C_2T_x$-4.0. The structure and physicochemical properties of PVA/$Ti_3C_2T_x$ MMMs were analyzed by scanning electron microscopy (SEM), energy dispersive spectrometry (EDS), atomic force microscopy (AFM), attenuated total reflectance-Fourier transform infrared spectroscopy (ATR-FTIR), X-ray diffraction (XRD), water contact angle (WCA), and degree of swelling (DS). In

https://dx.doi.org/10.1021/acsomega.9b03388
ACS Omega 2020, 5, 6277−6287

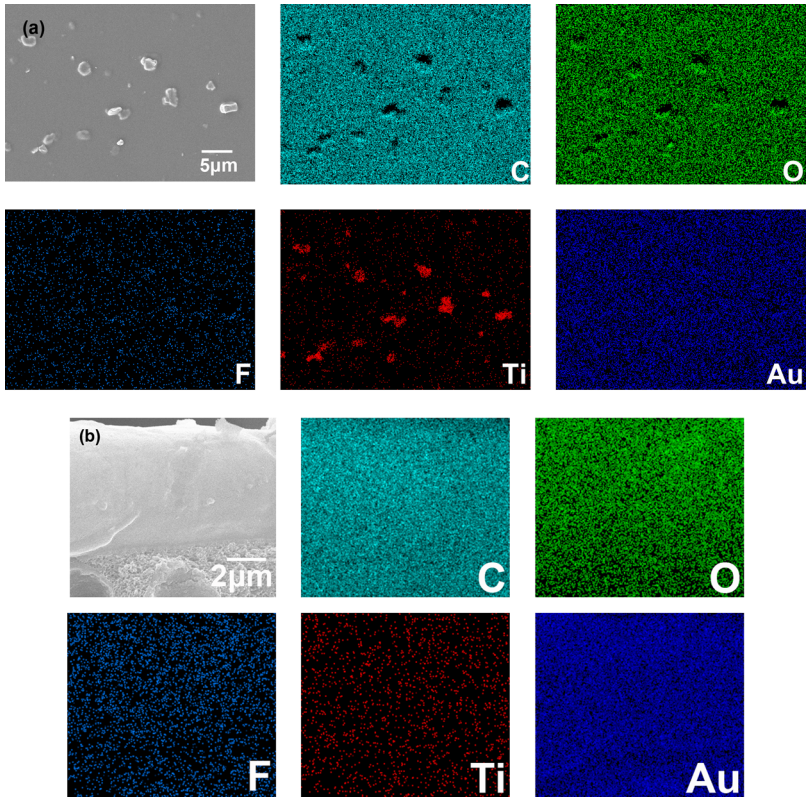

Figure 3. EDS results of PVA/$Ti_3C_2T_x$-3.0 MMMs: (a) surface view and (b) cross-sectional structure.

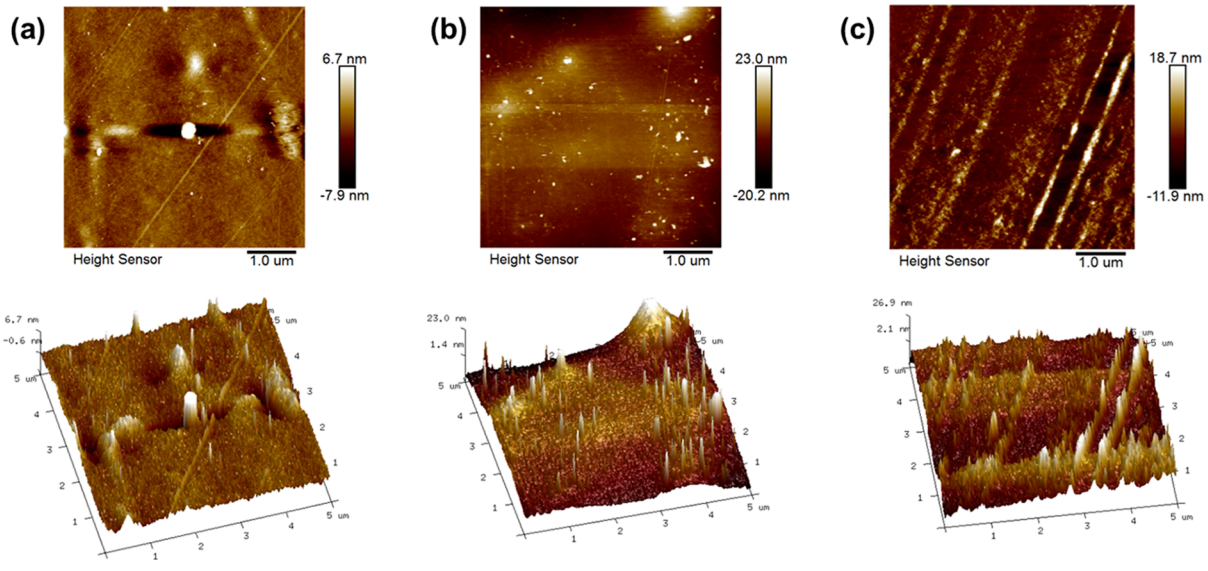

Figure 4. AFM images of PVA/$Ti_3C_2T_x$ MMMs with different mass fractions of $Ti_3C_2T_x$ filling: (a) 0.0; (b) 1.0; and (c) 3.0 wt %.

addition, the ethanol−water binary system was used to evaluate the PV performance of the PVA/$Ti_3C_2T_x$ MMMs.

2. RESULTS AND DISCUSSION

2.1. Morphology. The SEM morphology and EDS results of the $Ti_3C_2T_x$ powder are shown in Figure 1. The lateral dimension of $Ti_3C_2T_x$ was about 5 μm and showed a typical stacked layered structure like "accordion", which enabled $Ti_3C_2T_x$ advantageous for arranging 2D nanochannels in the PVA matrix.[41] It can be seen from the results of EDS analysis that $Ti_3C_2T_x$ mainly contained a large amount of Ti elements and C elements, and the presence of small quantities of Al elements may be because HF did not completely etch Al elements. In addition, 26.8 wt % of the O element and 9.5 wt % of the F element were observed, indicating that $Ti_3C_2T_x$ contained a large amount of oxygen functional groups, which was advantageous for improving the hydrophilicity of the material.

The surface and cross-sectional view of the PVA/$Ti_3C_2T_x$ MMMs are shown in Figure 2. As shown in Figure 2a−f, the surface image of the pristine PVA membrane was smooth and flat. The PVA/$Ti_3C_2T_x$ MMM surface with slight fluctuations

https://dx.doi.org/10.1021/acsomega.9b03388
ACS Omega 2020, 5, 6277−6287

looked dense without any visible defects. It indicates that $Ti_3C_2T_x$ has good compatibility with PVA, probably because of the interactions between the oxygen functional groups of $Ti_3C_2T_x$ and the PVA chain. In addition, it can be seen from Figure 3a that the surface of PVA/$Ti_3C_2T_x$-3.0 MMM is loaded with $Ti_3C_2T_x$ particles. Figure 2g–l showed the cross-sectional structure of the membranes, and the thickness of PVA/$Ti_3C_2T_x$ MMMs was about 6 μm. Moreover, the separation layer was firmly bonded on the PAN support layer.

The EDS diagram of surface morphology and cross-sectional structure of the PVA/$Ti_3C_2T_x$-3.0 MMM are shown in Figure 3. It can be seen that Ti elements and F elements are substantially uniformly distributed on the surface and cross section of the membrane, indicating that the distribution of $Ti_3C_2T_x$ in the PVA matrix is relatively uniform. Among them, the gold element is distributed by spraying gold during the sample preparation process.

To further research the surface structure of the MMMs, topography images and the surface roughness values of the MMMs were determined with AFM (Figure 4). The roughness values (R_a and R_q) of the membrane surface are shown in Table 1. The roughness increased with the increase of $Ti_3C_2T_x$ addition, which may be due to a higher $Ti_3C_2T_x$ filling that leads to a larger particle size with more chance of agglomeration on the membrane surface.

Table 1. Surface Roughness of the PVA/$Ti_3C_2T_x$ MMMs

surface roughness	PVA/$Ti_3C_2T_x$-0.0	PVA/$Ti_3C_2T_x$-1.0	PVA/$Ti_3C_2T_x$-3.0
R_a (nm)	1.99	4.02	4.87
R_q (nm)	2.58	5.49	6.31

2.2. ATR-FTIR and XRD Patterns of the Membranes. The ATR-FTIR patterns of $Ti_3C_2T_x$ powder, Ti_3AlC_2 powder, and PVA/$Ti_3C_2T_x$ MMMs are shown in Figure 5. As can be seen from Figure 5a, Ti_3AlC_2 is substantially free of any functional groups, whereas $Ti_3C_2T_x$ mainly comprises OH groups and C–O–C groups, which is consistent with previous articles.[33] In Figure 5b, the broad absorption peak at 3267 cm^{-1} represented the OH groups and the peak intensity of the PVA/$Ti_3C_2T_x$ MMMs at 3267 cm^{-1} decreased with increasing $Ti_3C_2T_x$ filling. The absorption bands at 1710 and 1234 cm^{-1} correspond to C=O and C–O groups, respectively. Moreover, the characteristic peak formed at 1090 cm^{-1} was related to the asymmetric stretching vibration of C–O–C groups. According to a previous study,[42] the cross-linking density of PVA/$Ti_3C_2T_x$ MMMs could be semi-quantitatively analyzed by the FT-IR peak intensity of C–O–C groups (1090 cm^{-1}) and OH group (3267 cm^{-1}) ratio (H_{1090}/H_{3267}). Table 2 demonstrated that the H_{1090}/H_{3267} increased with increasing $Ti_3C_2T_x$ filling. It further indicates that the cross-linking density of the PVA/$Ti_3C_2T_x$ MMMs is positively correlated with the amount of $Ti_3C_2T_x$ filling. The ATR-FTIR spectra showed that $Ti_3C_2T_x$ promoted the cross-linking reaction of PVA, and $Ti_3C_2T_x$ was well incorporated into the PVA matrix.

The Ti_3AlC_2 powder, $Ti_3C_2T_x$ powder, and PVA/$Ti_3C_2T_x$ MMMs were further studied by XRD. Figure 6a presented the XRD patterns of $Ti_3C_2T_x$ and Ti_3AlC_2 powders. $Ti_3C_2T_x$ powders were transferred to a lower angle at the (002) peak than Ti_3AlC_2, and $Ti_3C_2T_x$ has no strong diffraction peak at 2θ = 39°, which means that most of the Al elements on Ti_3AlC_2 were etched away and $Ti_3C_2T_x$ was successfully synthesized. The same conclusion appeared in previous reports.[34,37] In Figure 6b, a strong diffraction peak at 2θ = 19.7° (d-spacing of 4.5 Å) was a typical lattice of PVA, indicating that PVA is a semicrystalline polymer. The strong diffraction peaks of the PVA/$Ti_3C_2T_x$ MMMs at 2θ = 19.7° and 2θ = 8.4° represented the main characteristic peaks of PVA and $Ti_3C_2T_x$, respectively. In addition, with the increase of $Ti_3C_2T_x$ filling, the peak intensity at 2θ = 8.4° increased and the peak intensity at 2θ = 19.7° slightly decreased.

2.3. Hydrophilic and DS. The hydrophilicity of the membrane surface is an essential property for PV. Figure 7 shows the WCAs of different membranes. With the increase of $Ti_3C_2T_x$, the small decrease in contact angle indicates that the hydrophilicity is enhanced. Although with the increase of $Ti_3C_2T_x$ addition, the hydroxyl group is decreased, from Figure 4 and Table 1, we can see that the roughness is increased, and the combination of the two factors resulted in a small decrease in the contact angle.

The DS of the experiment was tested in water, pure ethanol, and 93 wt % ethanol aqueous solution at constant temperature. The DS formula is as the following equation

$$\mathrm{DS}\ \% = \left(\frac{W_A - W_B}{W_B}\right) \times 100 \quad (1)$$

where W_A and W_B are the mass of the wet and dry membrane samples (g), respectively. The DS of PVA/$Ti_3C_2T_x$ MMMs decreased with the increase of $Ti_3C_2T_x$ filling, as shown in Figure 8. The possible reason can be described that the

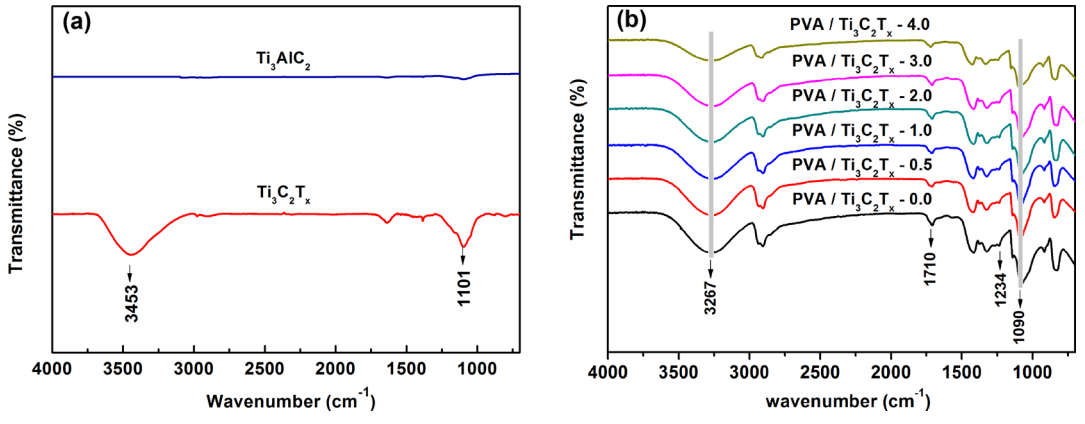

Figure 5. FT-IR spectra of (a) $Ti_3C_2T_x$, Ti_3AlC_2, and (b) PVA/$Ti_3C_2T_x$ MMMs.

https://dx.doi.org/10.1021/acsomega.9b03388
ACS Omega 2020, 5, 6277–6287

Table 2. Peak Intensity Ratio of 1090 and 3267 cm^{-1} in the FT-IR Spectra of PVA/$Ti_3C_2T_x$ MMMs

membrane	PVA/$Ti_3C_2T_x$-0.0	PVA/$Ti_3C_2T_x$-0.5	PVA/$Ti_3C_2T_x$-1.0	PVA/$Ti_3C_2T_x$-2.0	PVA/$Ti_3C_2T_x$-3.0	PVA/$Ti_3C_2T_x$-4.0
H_{1090}/H_{3267}	1.56	1.57	1.71	1.82	1.84	2.11

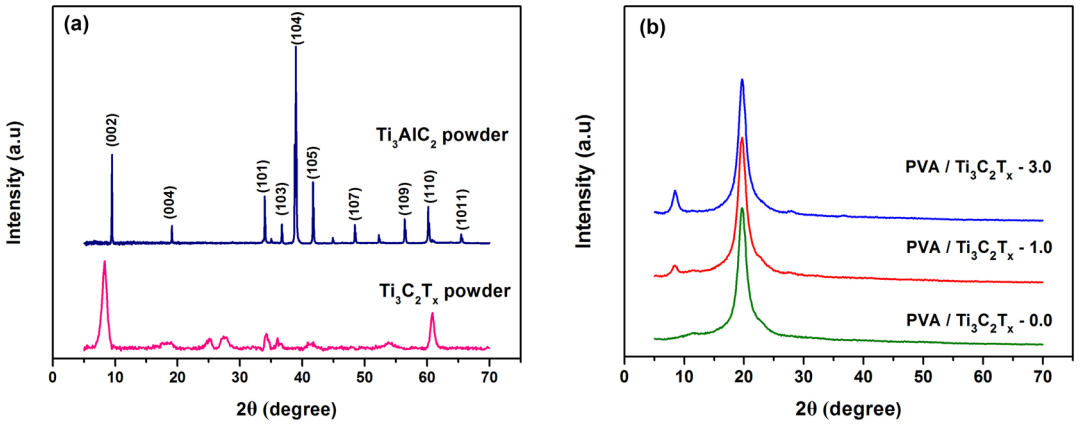

Figure 6. XRD patterns of Ti_3AlC_2 powder, $Ti_3C_2T_x$ powder, (a) and PVA/$Ti_3C_2T_x$ MMMs (b).

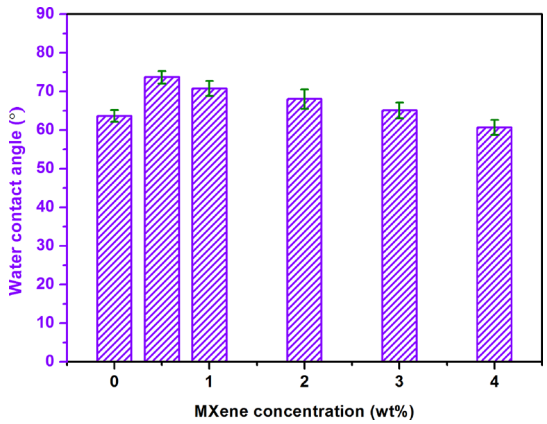

Figure 7. WCA of PVA/$Ti_3C_2T_x$ MMMs with different amounts of $Ti_3C_2T_x$ filling.

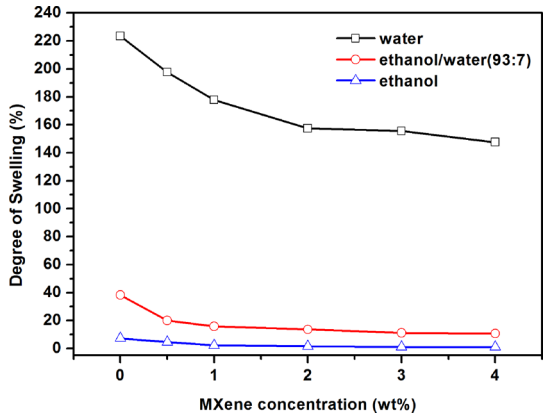

Figure 8. DS of PVA/$Ti_3C_2T_x$ MMMs with different $Ti_3C_2T_x$ loadings.

interaction between $Ti_3C_2T_x$ and the PVA matrix increases the cross-linking density of the membrane, which limits the movement of PVA molecular chains. In addition, the decrease of hydrophilicity of MMMs (Figure 7) results in a decrease of affinity for water molecules.[43] In general, $Ti_3C_2T_x$ has good mechanical properties and swelling resistance,[44] so the addition of $Ti_3C_2T_x$ inhibited the swelling of the PVA membrane.

2.4. PV Performance for the Ethanol−Water Binary System. The PV performance of PVA/$Ti_3C_2T_x$ MMMs for the ethanol−water binary system was evaluated. $Ti_3C_2T_x$ filling levels have a significant influence on the separation performance of the membrane. First, the effect of $Ti_3C_2T_x$ filling was studied at 37 °C and 93 wt % ethanol concentration. The total flux of PVA/$Ti_3C_2T_x$ MMMs decreased with increasing $Ti_3C_2T_x$ filling, as shown in Figure 9a. We can explain that the crystallinity of PVA membranes was not significantly improved (Figure 6) and the hydrophilicity of the membrane surface was declined (Figure 7) from the preceding analysis, which makes water molecules more difficult to enter the membranes. On the other hand, the resistance of water components passing through the membrane increases, attributed to the increase in the cross-linking density and aggregation of $Ti_3C_2T_x$, so the water flux decreased. The total flux depends on the water flux, so the total flux decreased. In addition, it can be seen that the water content in the permeate of the PVA/$Ti_3C_2T_x$ membranes exceeded 98.3 wt %. According to Figure 9b, the optimum value of the separation factor was 2585 when the $Ti_3C_2T_x$ filling was 3.0 wt %. Moreover, the separation factor increased when the $Ti_3C_2T_x$ loading increased from 0.0 to 3.0 wt %, which may be owing to the enhanced cross-linking density of PVA/$Ti_3C_2T_x$ MMMs, which led to the denser separation layer. The infrared analysis and DS test side demonstrated that the cross-linking density of the membrane increased after the addition of $Ti_3C_2T_x$. It showed that the addition of $Ti_3C_2T_x$ could improve the separation factor of the PVA membrane. However, when the amount of $Ti_3C_2T_x$ filling exceeded 3.0 wt %, the separation factor decreased, which may be due to the fact that $Ti_3C_2T_x$ loading reached the saturation limit, and higher than the concentration value, and agglomeration of $Ti_3C_2T_x$ occured, resulting in defects in the membrane.[41,43] Table 3 showed the effect of $Ti_3C_2T_x$ loading on the permeability and selectivity. Water permeability decreased with the increase of loading amount of $Ti_3C_2T_x$, and ethanol permeability first decreased and then increased. When the loading amount of $Ti_3C_2T_x$ was 3.0 wt %, ethanol permeability was the lowest. The PVA/

https://dx.doi.org/10.1021/acsomega.9b03388
ACS Omega 2020, 5, 6277−6287

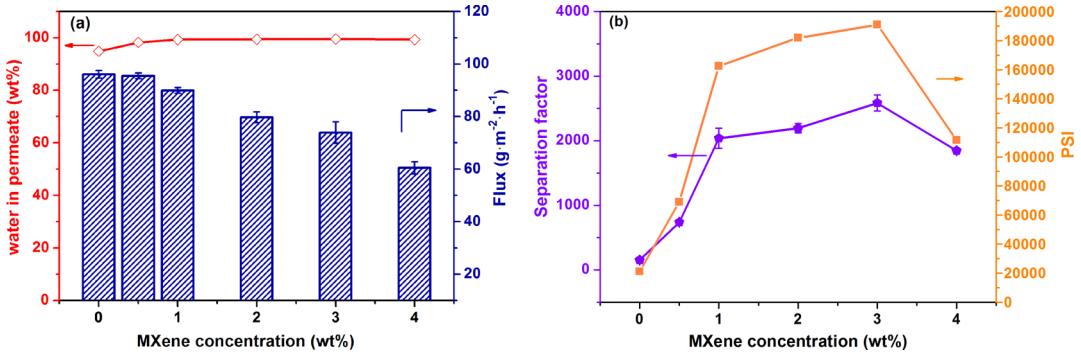

Figure 9. PV performance of PVA/$Ti_3C_2T_x$ MMMs. Total flux and water in the permeate (a) and separation factor and PSI (b) for membranes at different $Ti_3C_2T_x$ fillings.

Table 3. Effect of $Ti_3C_2T_x$ Loading on the Permeability and Selectivity

$Ti_3C_2T_x$ loading (wt %)	water permeability (10^6 g/m h kPa)	ethanol permeability (10^6 g/m h kPa)	total permeability (10^6 g/m h kPa)	selectivity
0.0	281.42	2.27	283.69	124.2
0.5	273.30	0.76	274.06	360.6
1.0	267.95	0.26	268.21	1006.4
2.0	237.63	0.21	237.84	1093.2
3.0	199.53	0.15	199.68	1298.3
4.0	160.01	0.20	160.21	826.5

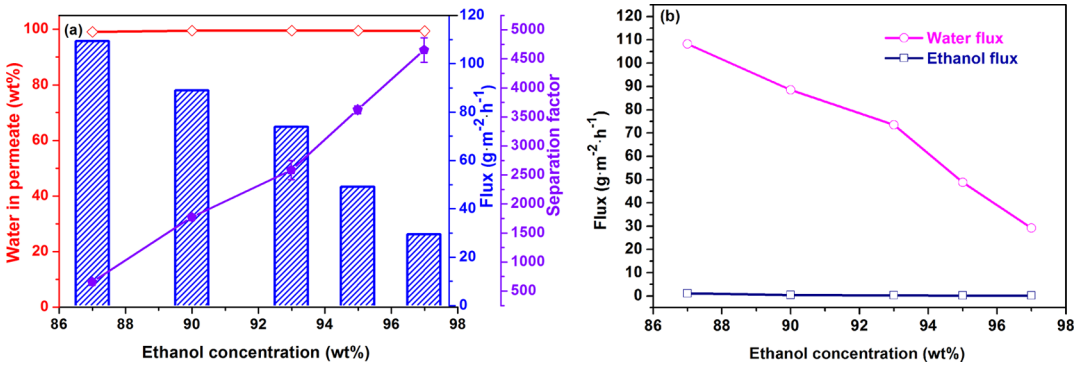

Figure 10. PV performance of the PVA/$Ti_3C_2T_x$-3.0 MMM. Total flux, water in permeates, and separation factor (a) and water flux and ethanol flux (b) for membranes at different feed concentrations.

Table 4. Effect of Ethanol Concentration on the Permeability and Selectivity of the PVA/$Ti_3C_2T_x$-3.0 MMM

ethanol concentration (wt %)	water permeability (10^6 g/m h kPa)	ethanol permeability (10^6 g/m h kPa)	total permeability (10^6 g/m h kPa)	selectivity
87	208.34	0.55	208.89	378.3
90	202.42	0.23	202.65	900.4
93	199.53	0.16	199.68	1298.3
95	196.02	0.10	196.12	1803.1
97	194.92	0.09	195.01	2304.2

$Ti_3C_2T_x$-3.0 MMM had the highest selectivity based on the change of water permeability and ethanol permeability, and this was consistent with the variation of the separation factor. The pervaporation separation index (PSI) is defined as the product of the total flux and separation factor and is used to characterize the PV performance of the membrane. PSI reached the highest value when the $Ti_3C_2T_x$ filling was 3.0 wt %. Herein, 3.0 wt % $Ti_3C_2T_x$ was the best filling amount for ethanol dehydration.

Based on the optimal $Ti_3C_2T_x$ filling, we evaluated the effect of ethanol concentration in the feed liquid for the PVA/$Ti_3C_2T_x$-3.0 MMM. The effect of the ethanol content in the feed solution on the PV performance at 37 °C is shown in Figure 10. The water concentration in the feed liquid directly affects the adsorption behavior of each component on the membrane surface. As shown in Figure 10a, when the ethanol concentration in the feed liquid increased from 87 to 97 wt %, the total flux decreased from 0.11 to 0.03 kg/m^2 h. This phenomenon was described in early work.[45] When the water content in the feed decreases, the selective interaction between water molecules and membranes decreases, which reduces the driving forces of the water molecules. Furthermore, from the result of the DS of the MMMs (Figure 8), at higher ethanol concentrations, the expansion degree of the membrane was less, which reduced the free volume of the membrane. Therefore, the transport resistance of ethanol and water

https://dx.doi.org/10.1021/acsomega.9b03388
ACS Omega 2020, 5, 6277−6287

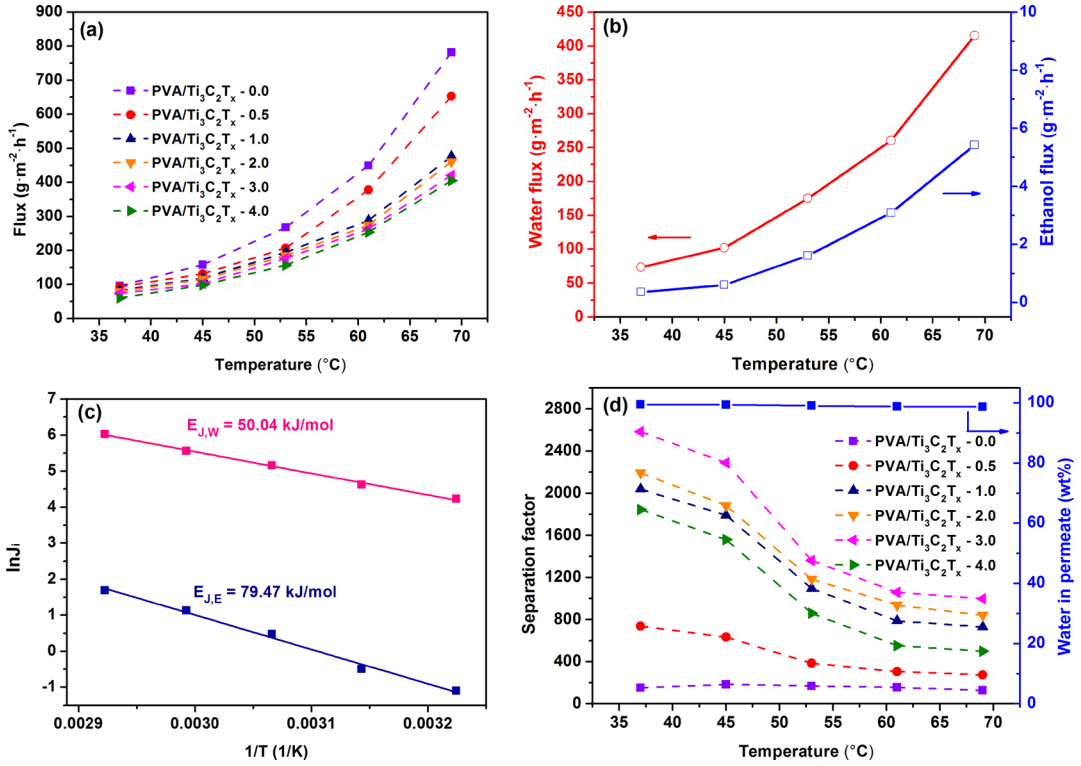

Figure 11. Total flux (a) and separation factor (d) of PVA/$Ti_3C_2T_x$ MMMs; water flux and ethanol flux (b), Arrhenius plots for water and ethanol flux (c), and water in permeates (d) of the PVA/$Ti_3C_2T_x$-3.0 membrane under varied temperature.

molecules increases, resulting in the decrease of total flux. It can be concluded from Figure 10b that the water flux was much higher than the ethanol flux, and the trend was close to the total flux, so the total flux was determined by the water flux. The information presented in Figure 10a also included that the separation factor increased from 654 to 4652 with the increase of ethanol concentration. This is mainly due to the decreases in the DS of the membrane, which weakens the chain movement of the polymer. Because of the large molecular diameter of ethanol and the difficulty of passing ethanol through the membrane, the adsorption selectivity of the membrane to water increases, resulting in an increase in the separation factor. At different feed concentrations, the water content in the permeate of the PVA/$Ti_3C_2T_x$-3.0 MMM exceeded 99 wt % (Figure 10a). The permeability and selectivity of the PVA/$Ti_3C_2T_x$-3.0 MMM at different ethanol concentrations in the feed liquid, as shown in Table 4, water permeability, and ethanol permeability increased with increasing ethanol concentration. The reason is that the DS of the membrane decreased with a decrease in water content, the free volume is reduced, and the diffusion of the components is limited.[25] In addition, the dissolution degree of the membrane is decreased, and then, the driving force of the molecules is reduced.[39] It is worth noting that the change in permeability is not significant, but the selectivity is significantly increased.

The influence of operation temperature on PV performance is special. Figure 11 showed the effect of operating temperature on the PV performance of PVA/$Ti_3C_2T_x$ MMMs at 93 wt % ethanol concentration. All of the PVA/$Ti_3C_2T_x$ MMMs showed significant enhancement in the total flux with increasing temperature, as shown in Figure 11a.[46] We attribute this phenomenon to two reasons: first, at high feed temperatures, free diffusion of ethanol and water molecules intensifies, which increases the free volume of molecules, and the activity of polymer segments promotes the increase of DS. Second, the vapor pressure on the feed side increases with increasing temperature, leading to an increase in the mass transfer driving force of the membrane. Moreover, as seen in Figure 11b, the water flux and ethanol flux of the PVA/$Ti_3C_2T_x$-3.0 MMM both increased with increasing temperature. Therefore, the total flux increased. The activation energies of water and ethanol were obtained using the Arrhenius diagram (Figure 11c). The variation of the permeation flux of each component follows the following equation

$$J = J_0 \exp\left(\frac{-E_a}{RT}\right) \quad (2)$$

where J is each component flux (kg/m^2 h), J_0 is the pre-exponential factor, R is the gas constant (kJ/mol K), E_p is the activation energy (kJ/mol), and T is the temperature. The activation energy of ethanol and water were 79.47 and 50.04 kJ/mol, respectively. The much higher ethanol activation energy indicated the higher temperature sensitivity of ethanol permeation over water permeation, and the ethanol flux tends to increase faster than that of water when the feed temperature increased. As shown in Figure 11d, the separation factor of all the PVA/$Ti_3C_2T_x$ MMMs decreased with increasing temperature, which was similar to previously reported dense PV membranes.[41,47] The reason was as follows: the free volume of molecules increases with increasing feed temperature, the permeation resistance of the ethanol molecules decreases, and furthermore, the penetration rate of ethanol exceeds the penetration rate of water. The permeability and selectivity of the PVA/$Ti_3C_2T_x$-3.0 MMM at different operating temperatures are shown in Table 5. It can be observed that the water

https://dx.doi.org/10.1021/acsomega.9b03388
ACS Omega 2020, 5, 6277−6287

Table 5. Effect of Temperature on the Permeability and Selectivity of the PVA/$Ti_3C_2T_x$-3.0 MMM

temperature (°C)	water permeability (10^6 g/m h kPa)	ethanol permeability (10^6 g/m h kPa)	total permeability (10^6 g/m h kPa)	selectivity	$E_{P,water}$ (kJ/mol)	$E_{P,ethanol}$ (kJ/mol)
37	199.53	0.15	199.68	1298.3	15.5	41.5
45	206.93	0.22	207.15	921.9		
53	220.27	0.33	220.60	661.5		
61	264.42	0.49	264.91	536.6		
69	300.56	0.68	301.24	441.4		

permeability and the ethanol permeability both increase with increasing temperature, and the increase in temperature promotes the diffusion process of the components, indicating that this is an endothermic process.[48] It is consistent with the trend of flux with temperature. The effect of temperature on permeability was described by the Arrhenius formula (eq 3)

$$P = P_0 \exp\left(\frac{-E_P}{RT}\right) \quad (3)$$

where P is each component permeability (10^6 g/m h kPa), P_0 is the pre-exponential factor, R is the gas constant (J/mol K), E_a is the activation energy (kJ/mol), and T is the temperature (K). Moreover, the permeability activation energies of water and ethanol are listed in Table 5. The smaller the apparent activation energy, the smaller the energy barrier of the molecule through the membrane,[48] where $E_{P,water}$ is less than $E_{P,ethanol}$, indicating that water permeability is more susceptible to temperature changes. In addition, because water permeability and ethanol permeability increase with increasing temperature, the selectivity of the membrane is decreased.[25] In addition, the water content in permeate of the PVA/$Ti_3C_2T_x$-3.0 MMM exceeded 99.5 wt % at 37 °C.

Figure 12 investigates the effect of operating time on the PV performance of the PVA/$Ti_3C_2T_x$-3.0 MMM. It can be seen

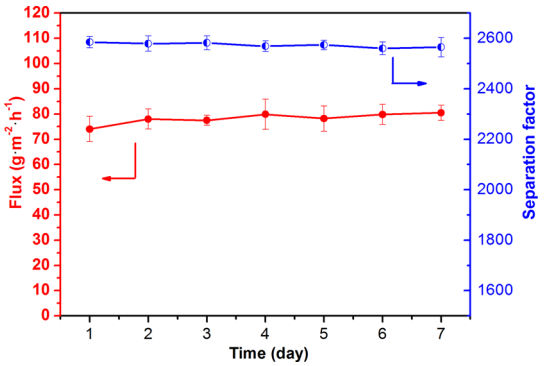

Figure 12. Long-term stability of the PVA/$Ti_3C_2T_x$-3.0 MMM under 37 °C and 93 wt % ethanol concentration.

that during continuous dehydration of the PVA/$Ti_3C_2T_x$-3.0 MMM at 37 °C and the 93 wt % ethanol−water binary mixture for about 7 days, the permeate flux and separation factor are relatively stable. It shows that the PVA/$Ti_3C_2T_x$ MMM can operate stably for a long time.

Table 6 listed the PV performance of PVA/$Ti_3C_2T_x$ MMMs for ethanol dehydration compared with reported membranes.[21,26,43,49−56] As can be seen, the prepared PVA/$Ti_3C_2T_x$ MMMs exhibited a higher separation factor than most PVA-based membranes. It is indicated that loading $Ti_3C_2T_x$ into polymer membranes has prospects.

Table 6. PV Performance of PVA-Based Membranes for the Ethanol−Water Binary System[a]

membr.	temp. (°C)	water content (wt %)	J (kg/m^2 h)	α	refs
PVA/C_3N_4	75	10	6.33	30.7	21
PVA/ZIF-8-NH_2	40	15	0.16	148	26
PVA/ZIF-90	30	10	0.27	1379	43
PVA/Fe-DA	30	10	0.99	2980	49
PVA/H-ZSM5	30	15	0.18	46	50
PVA/CF-TSA	50	30	0.13	775	51
PVA/NaY	60	20	0.30	450	52
PVA/SA	30	10	~0.35	25,000	53
PA/SDS-clay	25	10	12.0	0.28	54
SA/MoS_2	77	10	1.84	1229	55
CS/siloxane	25	10	0.47	2182	56
PVA	37	7	0.096	152	this work
PVA/$Ti_3C_2T_x$	37	7	0.074	2585	this work

[a]C_3N_4, carbon nitride; ZIF, zeolite imidazolate framework; Fe-DA, iron-dopamine nanoparticles; CF, carboxy fullerene; TSA, *p*-toluene sulfonic acid; ZSM, molecular sieve; NaY, molecular sieve; SA, sodium alginate; PA, polyamide; MoS_2, molybdenum disulphide; CS, chitosan.

3. CONCLUSIONS

In this study, the novel two-dimensional material, $Ti_3C_2T_x$, was used as an inorganic filler to prepare PVA/$Ti_3C_2T_x$ MMMs. GA and PAN ultrafiltration membranes were used as cross-linking agents and the support layer, respectively. The results showed that $Ti_3C_2T_x$ could be uniformly dispersed in the PVA matrix, and they had excellent compatibility. In addition, PVA/$Ti_3C_2T_x$ MMMs exhibited excellent mechanical properties and swelling resistance. PV performance results showed that loading $Ti_3C_2T_x$ in the PVA matrix significantly improved the separation factor of PVA membranes, but the total flux of PVA membranes decreased because of the enhanced cross-linking density and the weakened hydrophilicity of the membrane surface. The PVA/$Ti_3C_2T_x$-3.0 MMM had the best PV performance at 37 °C and 93 wt % ethanol solution, and the separation factor was 2585, which was 17 times higher than that of the pristine PVA membrane and with an acceptable permeation flux of 0.074 kg/m^2 h. When the concentration of ethanol decreased and the feed temperature increased, the separation factor decreased and the total flux increased significantly, which was consistent with the typical regular of polymer membranes. The newly developed PVA/$Ti_3C_2T_x$ MMMs have great potential for membrane separation applications, which provide some reference for the application of $Ti_3C_2T_x$ in PV.

https://dx.doi.org/10.1021/acsomega.9b03388
ACS Omega 2020, 5, 6277−6287

4. EXPERIMENTAL SECTION

4.1. Materials. PVA-124 was purchased from Xilong Chemical Co., Ltd. (Guangdong, China). Lithium fluoride (LiF, >99.9%) was supplied by Shanghai Macklin Biochemical Co., Ltd. (Shanghai, China). Hydrochloric acid (HCl, AR) was from Beijing Chemical Works (Beijing, China). Glutaraldehyde (GA, 50%) was obtained from Tianjin Guangfu Fine Chemical Research Institute. (Tianjin, China). Glacial acetic acid (HAc, AR) and ethanol (AR) were purchased from Sinopharm Chemical Reagent Co., Ltd. (Shanghai, China).

4.2. Synthesis of $Ti_3C_2T_x$ Powders. LiF and HCl were used as milder etchants to replace HF, which were similar to previous research.[31,33] The procedure was as follows: 1.98 g of LiF was slowly added to 6 M HCl solution (30 mL). After magnetic stirring for 1 h, 3 g of Ti_3AlC_2 powder was slowly added to the solution, and then, the mixture was held at 40 °C for 45 h and centrifuged with deionized water until the supernatant reached neutrality. Then, the black powder was dispersed in deionized water and sonicated for 1 h. Thereafter, the solution was centrifuged for 1 h to remove large particles. After decantation, the black $Ti_3C_2T_x$ colloidal supernatants were obtained and dried in a vacuum oven.

4.3. Fabrication of PVA/$Ti_3C_2T_x$ MMMs. First, 8 g of PVA powders was dissolved in 2 wt % HAc solution (92 g) and stirred for 1 h at 90 °C, and then, the insoluble large particles were filtered off. An amount of $Ti_3C_2T_x$ powder was dispersed in deionized water and sonicated for 1 h. Moreover, the abovementioned solutions were mixed and sonicated for 0.5 h to form uniform dispersions. GA (2 wt %) was added as a cross-linking agent to prepare the casting solution. Next, the casting solution was degassed by vacuum and poured onto the PAN ultrafiltration membranes, and solvents evaporate in a fume hood for 12 h. Finally, PVA/$Ti_3C_2T_x$ MMMs were prepared by cross-linking for 2 h in an electric drying oven at 90 °C.

4.4. Evaluation of the PV Performance Test. The schematic diagram of the self-designed PV apparatus is illustrated in Figure 13. Among them, the effective area of the membrane was 2.2×10^{-3} m^2. The pump delivers the feed liquid to the membrane cell. The vacuum on the permeate side is formed using a vacuum pump, and the minimum absolute pressure can reach 0.2 kPa. The permeation mixture was collected in the cold trap made of liquid nitrogen bath, and the contents of upstream feed solution and downstream permeate were analyzed by gas chromatography (Shimadzu, GC-14C, Japan).

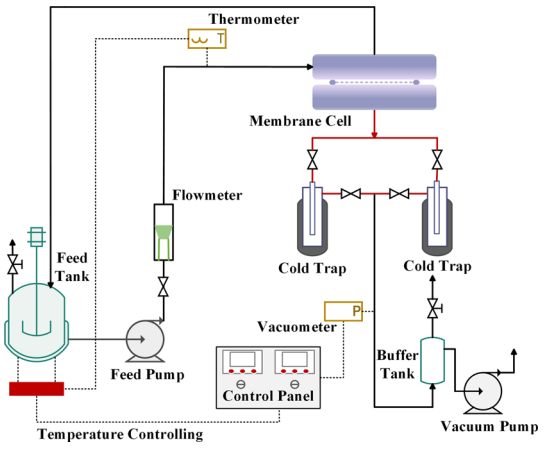

Figure 13. Schematic illustration of the PV evaluation apparatus.

The total flux (J) and separation factor (α) were two key indicators of PV performances, which are defined as the following equations

$$J = \frac{Q}{A \cdot t} \tag{4}$$

$$\alpha = \frac{Y_i/Y_j}{X_i/X_j} \tag{5}$$

where J is the total flux (kg/m^2 h); Q is the weight of the permeation component (g); A is the effective area of the membrane (m^2); t is the time (h); α represents the separation factor; Y is the mass fraction of components in the permeate liquid (wt %); X is the mass fraction of components in the feed liquid (wt %); and i and j stand for water and ethanol, respectively.

In addition, the permeability (P_i) and the selectivity (β_P) are defined as eqs 6 and 7

$$P_i = \frac{J_i \times l}{x_i \gamma_i P_i^s - y_i P^P} \tag{6}$$

$$\beta_P = \frac{P_W}{P_E} \tag{7}$$

where P_i is each component permeability (10^6 g/m h kPa), J_i is each component flux (kg/m^2 h), l is the thickness of the separation layer (m), x and y stand for the molar fractions of the component in the feed liquid and the permeate liquid (%), respectively, γ_i and P_i^s (kPa) are the activity coefficients of feed mixtures and saturated vapor pressures obtained using Aspen Plus software, P^P is the permeate side pressure (kPa), β_P is the selectivity, and P_W and P_E are water permeability and ethanol permeability (10^6 g/m h kPa), respectively.

4.5. Characterization. The morphology of powder and membranes was characterized by SEM (JSM7401F, Japan) and EDS. AFM (SPA-400, Japan) was used to characterize the morphology of membranes. The structural properties of PVA/$Ti_3C_2T_x$ MMMs were studied with ATR-FTIR (Bruker TENSOR 27). The diffraction patterns and crystalline phases of membranes (remove the PAN ultrafiltration membrane) were researched by XRD (Bruker D8 ADVANCE, Germany). The Ti_3AlC_2 and $Ti_3C_2T_x$ powders were also characterized. The hydrophilicity of membranes was experimented by the WCA (Model PV-DP). The DS test was also performed.

AUTHOR INFORMATION

Corresponding Author

Weibin Cai − *School of Chemical and Environmental Engineering, China University of Mining and Technology, Beijing 100083, China;* orcid.org/0000-0002-7967-2699; Email: caiweibin@tsinghua.org.cn

Authors

Xue Cheng − *School of Chemical and Environmental Engineering, China University of Mining and Technology, Beijing 100083, China*

Xiaohan Chen − *School of Chemical and Environmental Engineering, China University of Mining and Technology, Beijing 100083, China*

https://dx.doi.org/10.1021/acsomega.9b03388
ACS Omega 2020, 5, 6277−6287

Jiding Li − *Department of Chemical Engineering, Tsinghua University, Beijing 100084, China*
Junqi Pei − *School of Chemical and Environmental Engineering, China University of Mining and Technology, Beijing 100083, China*

Complete contact information is available at: https://pubs.acs.org/10.1021/acsomega.9b03388

Notes

The authors declare no competing financial interest.

■ ACKNOWLEDGMENTS

This work has been financially supported by the National Natural Science Foundation of China (nos. 21736001, 21776153, and 21576150).

■ REFERENCES

(1) Kumar, S.; Singh, N.; Prasad, R. Anhydrous ethanol: A renewable source of energy. *Renewable Sustainable Energy Rev.* **2010**, *14*, 1830−1844.
(2) Cardona, C. A.; Sánchez, Ó. J. Fuel ethanol production: Process design trends and integration opportunities. *Bioresour. Technol.* **2007**, *98*, 2415−2457.
(3) Srivastava, N.; Rawat, R.; Singh Oberoi, H.; Ramteke, P. W. A Review on Fuel Ethanol Production From Lignocellulosic Biomass. *Int. J. Green Energy* **2015**, *12*, 949−960.
(4) Kober, P. A. Pervaporation, perstillation and percrystallization. *J. Am. Chem. Soc.* **1917**, *39*, 944−948.
(5) Bolto, B.; Hoang, M.; Xie, Z. A review of membrane selection for the dehydration of aqueous ethanol by pervaporation. *Chem. Eng. Process.* **2011**, *50*, 227−235.
(6) Liu, G.; Wei, W.; Jin, W. Pervaporation Membranes for Biobutanol Production. *ACS Sustainable Chem. Eng.* **2014**, *2*, 546−560.
(7) Neto, J. M.; Pinho, M. N. Mass transfer modelling for solvent dehydration by pervaporation. *Sep. Purif. Technol.* **2000**, *18*, 151−161.
(8) Shaban, H. I. Pervaporation separation of water from organic mixtures. *Sep. Purif. Technol.* **1997**, *11*, 119−126.
(9) Anjali Devi, D.; Smitha, B.; Sridhar, S.; Aminabhavi, T. M. Pervaporation separation of isopropanol/water mixtures through crosslinked chitosan membranes. *J. Membr. Sci.* **2005**, *262*, 91−99.
(10) Chen, J. H.; Liu, Q. L.; Zhu, A. M.; Zhang, Q. G. Dehydration of acetic acid by pervaporation using SPEK-C/PVA blend membranes. *J. Membr. Sci.* **2008**, *320*, 416−422.
(11) Dudek, G.; Turczyn, R.; Gnus, M.; Konieczny, K. Pervaporative dehydration of ethanol/water mixture through hybrid alginate membranes with ferroferic oxide nanoparticles. *Sep. Purif. Technol.* **2018**, *193*, 398−407.
(12) Choudhury, S.; Ray, S. K. Filled copolymer membranes for pervaporative dehydration of ethanol-water mixture. *Sep. Purif. Technol.* **2017**, *179*, 335−348.
(13) Gimenes, M. L.; Liu, L.; Feng, X. Sericin/poly(vinyl alcohol) blend membranes for pervaporation separation of ethanol/water mixtures. *J. Membr. Sci.* **2007**, *295*, 71−79.
(14) Vijayakumarnaidu, B.; Sairam, M.; Raju, K.; Aminabhavi, T. M. Pervaporation separation of water plus isopropanol mixtures using novel nanocomposite membranes of poly(vinyl alcohol) and polyaniline. *J. Membr. Sci.* **2005**, *260*, 142−155.
(15) Doguparthy, S. Pervaporation of aqueous alcohol mixtures through a photopolymerised composite membrane. *J. Membr. Sci.* **2001**, *185*, 201−205.
(16) Cheng, P.-I.; Hong, P.-D.; Lee, K.-R.; Lai, J.-Y.; Tsai, Y.-L. High permselectivity of networked PVA/GA/CS-Ag^+-membrane for dehydration of Isopropanol. *J. Membr. Sci.* **2018**, *564*, 926−934.
(17) Khoonsap, S.; Supanchaiyamat, N.; Hunt, A. J.; Klinsrisuk, S.; Amnuaypanich, S. Improving water selectivity of poly (vinyl alcohol) (PVA) - Fumed silica (FS) nanocomposite membranes by grafting of poly (2-hydroxyethyl methacrylate) (PHEMA) on fumed silica particles. *Chem. Eng. Sci.* **2015**, *122*, 373−383.
(18) Butler, S. Z.; Hollen, S. M.; Cao, L.; Cui, Y.; Gupta, J. A.; Gutiérrez, H. R.; Heinz, T. F.; Hong, S. S.; Huang, J.; Ismach, A. F.; Johnston-Halperin, E.; Kuno, M.; Plashnitsa, V. V.; Robinson, R. D.; Ruoff, R. S.; Salahuddin, S.; Shan, J.; Shi, L.; Spencer, M. G.; Terrones, M.; Windl, W.; Goldberger, J. E. Progress, Challenges, and Opportunities in Two-Dimensional Materials Beyond Graphene. *ACS Nano* **2013**, *7*, 2898−2926.
(19) Geim, A. K.; Novoselov, K. S. The rise of graphene. *Nat. Mater.* **2007**, *6*, 183−191.
(20) Zhu, Y.; Murali, S.; Cai, W.; Li, X.; Suk, J. W.; Potts, J. R.; Ruoff, R. S. Graphene and Graphene Oxide: Synthesis, Properties, and Applications. *Adv. Mater.* **2010**, *22*, 3906−3924.
(21) Wang, J.; Li, M.; Zhou, S.; Xue, A.; Zhang, Y.; Zhao, Y.; Zhong, J.; Zhang, Q. Graphitic carbon nitride nanosheets embedded in poly(vinyl alcohol) nanocomposite membranes for ethanol dehydration via pervaporation. *Sep. Purif. Technol.* **2017**, *188*, 24−37.
(22) Wang, Y.; Li, L.; Wei, Y.; Xue, J.; Chen, H.; Ding, L.; Caro, J.; Wang, H. Water Transport with Ultralow Friction through Partially Exfoliated g-C_3N_4 Nanosheet Membranes with Self-Supporting Spacers. *Angew. Chem., Int. Ed.* **2017**, *56*, 8974−8980.
(23) Kasik, A.; Lin, Y. S. Organic solvent pervaporation properties of MOF-5 membranes. *Sep. Purif. Technol.* **2014**, *121*, 38−45.
(24) Mak, K. F.; Lee, C.; Hone, J.; Shan, J.; Heinz, T. F. Atomically Thin MoS_2: A New Direct-Gap Semiconductor. *Phys. Rev. Lett.* **2010**, *105*, 666.
(25) Wu, G.; Li, Y.; Geng, Y.; Lu, X.; Jia, Z. Adjustable pervaporation performance of Zr-MOF/poly(vinyl alcohol) mixed matrix membranes. *J. Chem. Technol. Biotechnol.* **2019**, *94*, 973−981.
(26) Zhang, H.; Wang, Y. Poly(vinylalcohol)/ZIF-8-NH_2 Mixed Matrix Membranes for Ethanol Dehydration via Pervaporation. *AIChE J.* **2016**, *62*, 1728−1739.
(27) Kim, T.; Lee, J.; Lee, G.; Lee, J.; Song, H.; Jho, J. Y.; Lee, H. H.; Kim, Y. H. Synthesis of a Carbonaceous Two-Dimensional (2D) Material. *ACS Appl. Mater. Interfaces* **2019**, *11*, 21308−21313.
(28) Liu, G.; Jin, W.; Xu, N. Two-Dimensional-Material Membranes: A New Family of High-Performance Separation Membranes. *Angew. Chem., Int. Ed.* **2016**, *55*, 13384−13397.
(29) Zhuang, X.; Mai, Y.; Wu, D.; Zhang, F.; Feng, X. Two-Dimensional Soft Nanomaterials: A Fascinating World of Materials. *Adv. Mater.* **2015**, *27*, 403−427.
(30) Huang, L.; Lin, H. Engineering Sub-Nanometer Channels in Two-Dimensional Materials for Membrane Gas Separation. *Membr* **2018**, *8*, 100.
(31) Naguib, M.; Kurtoglu, M.; Presser, V.; Lu, J.; Niu, J.; Heon, M.; Hultman, L.; Gogotsi, Y.; Barsoum, M. W. Two-Dimensional Nanocrystals Produced by Exfoliation of Ti_3AlC_2. *Adv. Mater.* **2011**, *23*, 4248−4253.
(32) Naguib, M.; Halim, J.; Lu, J.; Cook, K. M.; Hultman, L.; Gogotsi, Y.; Barsoum, M. W. New Two-Dimensional Niobium and Vanadium Carbides as Promising Materials for Li-Ion Batteries. *J. Am. Chem. Soc.* **2013**, *135*, 15966−15969.
(33) Ghidiu, M.; Lukatskaya, M. R.; Zhao, M.-Q.; Gogotsi, Y.; Barsoum, M. W. Conductive two-dimensional titanium carbide 'clay' with high volumetric capacitance. *Nat* **2014**, *516*, 78−81.
(34) Ding, L.; Wei, Y.; Wang, Y.; Chen, H.; Caro, J.; Wang, H. A Two-Dimensional Lamellar Membrane: MXene Nanosheet Stacks. *Angew. Chem., Int. Ed.* **2017**, *56*, 1825−1829.
(35) Ren, C. E.; Hatzell, K. B.; Alhabeb, M.; Ling, Z.; Mahmoud, K. A.; Gogotsi, Y. Charge- and Size-Selective Ion Sieving Through $Ti_3C_2T_x$ MXene Membranes. *J. Phys. Chem. Lett.* **2015**, *6*, 4026−4031.
(36) Xu, Z.; Sun, Y.; Zhuang, Y.; Jing, W.; Ye, H.; Cui, Z. Assembly of 2D MXene nanosheets and TiO_2 nanoparticles for fabricating mesoporous TiO_2-MXene membranes. *J. Membr. Sci.* **2018**, *564*, 35−43.
(37) Liu, G.; Shen, J.; Liu, Q.; Liu, G.; Xiong, J.; Yang, J.; Jin, W. Ultrathin two-dimensional MXene membrane for pervaporation desalination. *J. Membr. Sci.* **2018**, *548*, 548−558.

(38) Wu, Y.; Ding, L.; Lu, Z.; Deng, J.; Wei, Y. Two-dimensional MXene membrane for ethanol dehydration. *J. Membr. Sci.* **2019**, *590*, 117300.
(39) Ding, L.; Wei, Y.; Li, L.; Zhang, T.; Wang, H.; Xue, J.; Ding, L.-X.; Wang, S.; Caro, J.; Gogotsi, Y. MXene molecular sieving membranes for highly efficient gas separation. *Nat. Commun.* **2018**, *9*, 155−161.
(40) Li, L.; Zhang, T.; Duan, Y.; Wei, Y.; Dong, C.; Ding, L.; Qiao, Z.; Wang, H. Selective gas diffusion in two-dimensional MXene lamellar membranes: insights from molecular dynamics simulations. *J. Mater. Chem. A* **2018**, *6*, 11734−11742.
(41) Xu, Z.; Liu, G.; Ye, H.; Jin, W.; Cui, Z. Two-dimensional MXene incorporated chitosan mixed-matrix membranes for efficient solvent dehydration. *J. Membr. Sci.* **2018**, *563*, 625−632.
(42) Liu, Y.; Zhu, M.; Zhao, Q.; An, Q.; Qian, J.; Lee, K.; Lai, J. The chemical crosslinking of polyelectrolyte complex colloidal particles and the pervaporation performance of their membranes. *J. Membr. Sci.* **2011**, *385*−*386*, 132−140.
(43) Wei, Z.; Liu, Q.; Wu, C.; Wang, H.; Wang, H. Viscosity-driven in situ self-assembly strategy to fabricate cross-linked ZIF-90/PVA hybrid membranes for ethanol dehydration via pervaporation. *Sep. Purif. Technol.* **2018**, *201*, 256−267.
(44) Lu, Z.; Wei, Y.; Deng, J.; Ding, L.; Li, Z.-K.; Wang, H. Self-Crosslinked MXene ($Ti_3C_2T_x$) Membranes with Good Antiswelling Property for Monovalent Metal Ion Exclusion. *ACS Nano* **2019**, *13*, 10535−10544.
(45) Cheng, X.; Cai, W.; Chen, X.; Shi, Z.; Li, J. Preparation of graphene oxide/poly(vinyl alcohol) composite membrane and pervaporation performance for ethanol dehydration. *RSC Adv.* **2019**, *9*, 15457−15465.
(46) He, X.; Wang, T.; Li, Y.; Chen, J.; Li, J. Fabrication and characterization of micro-patterned PDMS composite membranes for enhanced ethanol recovery. *J. Membr. Sci.* **2018**, *563*, 447−459.
(47) Ong, Y. K.; Shi, G. M.; Le, N. L.; Tang, Y. P.; Zuo, J.; Nunes, S. P.; Chung, T.-S. Recent membrane development for pervaporation processes. *Prog. Polym. Sci.* **2016**, *57*, 1−31.
(48) Narkkun, T.; Jenwiriyakul, W.; Amnuaypanich, S. Dehydration performance of double-network poly(vinyl alcohol) nanocomposite membranes (PVAs-DN). *J. Membr. Sci.* **2017**, *528*, 284−295.
(49) Liu, Q.; Wang, H.; Wu, C.; Wei, Z.; Wang, H. In-situ generation of iron-dopamine nanoparticles with hybridization and cross-linking dual-functions in poly (vinyl alcohol) membranes for ethanol dehydration via pervaporation. *Sep. Purif. Technol.* **2017**, *188*, 282−292.
(50) Suhas, D. P.; Aminabhavi, T. M.; Raghu, A. V. Mixed Matrix Membranes of H-ZSM5-Loaded Poly(vinyl alcohol) Used in Pervaporation Dehydration of Alcohols: Influence of Silica/Alumina Ratio. *Polym. Eng. Sci.* **2014**, *54*, 1774−1782.
(51) Penkova, A. V.; Dmitrenko, M. E.; Savon, N. A.; Missyul, A. B.; Mazur, A. S.; Kuzminova, A. I.; Zolotarev, A. A.; Mikhailovskii, V.; Lahderanta, E.; Markelov, D. A.; Semenov, K. N.; Ermakov, S. S. Novel mixed-matrix membranes based on polyvinyl alcohol modified by carboxyfullerene for pervaporation dehydration. *Sep. Purif. Technol.* **2018**, *204*, 1−12.
(52) Huang, Z.; Guan, H.; Tan, W.; Qiao, X.; Kulprathipanja, S. Pervaporation study of aqueous ethanol solution through zeolite-incorporated multilayer poly(vinyl alcohol) membranes: Effect of zeolites. *J. Membr. Sci.* **2006**, *276*, 260−271.
(53) Yeom, C. K.; Lee, S. H.; Lee, J. M. Pervaporative permeations of homologous series of alcohol aqueous mixtures through a hydrophilic membrane. *J. Appl. Polym. Sci.* **2001**, *79*, 703−713.
(54) Wang, Y.-C.; Fan, S.-C.; Lee, K.-R.; Li, C.-L.; Huang, S.-H.; Tsai, H.-A.; Lai, J.-Y. Polyamide/SDS-clay hybrid nanocomposite membrane application to water-ethanol mixture pervaporation separation. *J. Membr. Sci.* **2004**, *239*, 219−226.
(55) Song, Y.; Jiang, Z.; Gao, B.; Wang, H.; Wang, M.; He, Z.; Cao, X.; Pan, F. Embedding hydrophobic MoS_2 nanosheets within hydrophilic sodium alginate membrane for enhanced ethanol dehydration. *Chem. Eng. Sci.* **2018**, *185*, 231−242.
(56) Lin, Y.-F.; Ho, J.-C.; Andrew Lin, K.-Y.; Tung, K.-L.; Chung, T.-W.; Lee, C.-C. A drying-free and one-step process for the preparation of siloxane/CS mixed-matrix membranes with outstanding ethanol dehydration performances. *Sep. Purif. Technol.* **2019**, *221*, 325−330.

https://dx.doi.org/10.1021/acsomega.9b03388
ACS Omega 2020, 5, 6277−6287